

Capturing Turbulent Dynamics and Statistics in Experiments with Unstable Periodic Orbits

Balachandra Suri,^{1,*} Logan Kageorge², Roman O. Grigoriev^{2,†} and Michael F. Schatz^{2,‡}

¹IST-Austria, 3400 Klosterneuburg, Austria

²School of Physics, Georgia Institute of Technology, Atlanta, Georgia 30332, USA

 (Received 31 December 2019; revised 19 May 2020; accepted 5 July 2020; published 5 August 2020)

In laboratory studies and numerical simulations, we observe clear signatures of unstable time-periodic solutions in a moderately turbulent quasi-two-dimensional flow. We validate the dynamical relevance of such solutions by demonstrating that turbulent flows in both experiment and numerics transiently display time-periodic dynamics when they shadow unstable periodic orbits (UPOs). We show that UPOs we computed are also statistically significant, with turbulent flows spending a sizable fraction of the total time near these solutions. As a result, the average rates of energy input and dissipation for the turbulent flow and frequently visited UPOs differ only by a few percent.

DOI: [10.1103/PhysRevLett.125.064501](https://doi.org/10.1103/PhysRevLett.125.064501)

Characteristic flow patterns (coherent structures) embedded in turbulence play critical roles in both moderately [1] and highly turbulent flows [2,3], including cascade processes in two and three dimensions [4–6]. However, inherently statistical descriptions of turbulence, which are currently widely accepted, fail to describe coherent structures effectively. Consequently, they are unable to quantitatively predict statistical averages of turbulent flows (e.g., energy dissipation rates).

Recent studies suggest that coherent structures in turbulence can be described by *recurrent* (e.g., time-periodic) solutions to the deterministic equations governing fluid flow [1,7–11]. The existence of such solutions embedded within a chaotic set suggests the possibility of a fundamentally dynamical theory, inspired by Hopf’s vision of turbulence as a walk between neighborhoods of recurrent solutions [8,12]. For certain (e.g., uniformly hyperbolic) low-dimensional dynamical systems exhibiting chaos, this viewpoint has been fleshed out; chaotic trajectories in state space *shadow* (follow) a dense set of recurrent solutions in the form of unstable time-periodic orbits (UPOs). This property enables short-time forecasting and the computation [via periodic orbit theory (POT)] of statistical averages from properly weighted sums evaluated over UPOs, with higher weights assigned to more frequently visited UPOs [13–15].

Although the equations governing turbulence are formally infinite dimensional, turbulent flows (due to dissipation) can be represented as state space trajectories confined to finite-dimensional chaotic sets [12]. This dimension can be estimated, e.g., based on the number of unstable directions of UPOs and can be relatively low [$O(10)$] for transitional flows in domains of moderate size [16–19]. While this qualitative similarity with low-dimensional chaos is encouraging, variability in the number

of unstable directions for UPOs suggests turbulent flows are nonhyperbolic [20]. The stable and unstable manifolds of dynamically invariant sets become tangent at some locations inside the chaotic set, destroying the shadowing property there and raising questions regarding the utility of UPOs for both forecasting and computing statistical averages.

To date, research devoted to developing and testing a dynamical description of turbulence based on UPOs has relied exclusively on direct numerical simulations (DNS) [5,7,10,18,21–27]. Despite the likely presence of non-hyperbolicity, studies focusing on transitional flows (with dynamics and statistics dominated by coherent structures) have generated valuable new insight. In canonical three-dimensional shear flows (e.g., plane Couette) it was shown that UPOs capture salient dynamical aspects (e.g., self-sustaining processes [28]) and statistical averages (e.g., mean flow profile) of turbulent flows [5,7,10,21,22]. However, definitive evidence in support of POT has not emerged even from studies that identified large sets of (≈ 50) UPOs [17,29].

Previous numerical studies have imposed numerous flow restrictions, including spatially periodic boundary conditions, minimal-flow-unit domains and symmetry invariance, that are not representative of experiment. Consequently, direct experimental evidence for shadowing—turbulent flows approaching UPOs and mimicking their *spatiotemporal* evolution—has not been reported previously. Also, some amount of noise is always present in experiments and how it affects the dynamical relevance of UPOs is not currently understood. Lastly, the statistical significance of UPOs in laboratory flows is also an outstanding question.

In this Letter, we report clear evidence of UPOs in an experimental quasi-two-dimensional (quasi-2D) flow, in a

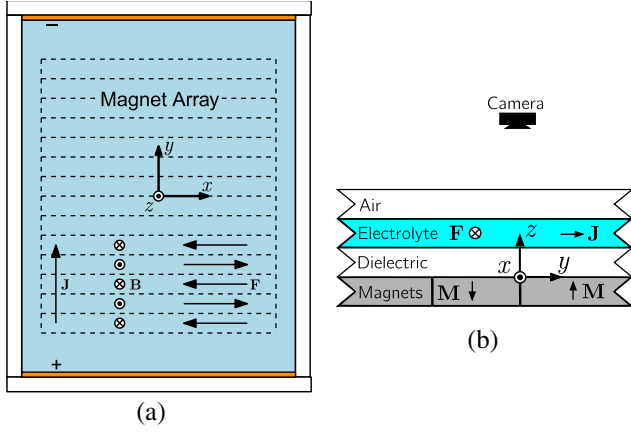


FIG. 1. Experimental setup to generate quasi-2D Kolmogorov-like flow. (a) Top view indicating magnet array (dashed lines) and directions of magnetic field \mathbf{B} , current density $\mathbf{J} = J\hat{y}$, and electromagnetic forcing \mathbf{F} . (b) Side view showing stably stratified immiscible two-layer configuration.

domain whose size is much larger than a minimal flow unit. DNS of this moderately turbulent (transitional) flow is performed with no-slip boundary conditions and without imposing any symmetry constraints. In particular, to test the shadowing hypothesis, we study the spatiotemporal evolution of turbulent flows that approach UPOs closely. We investigate the relation between statistical “weights” predicted by POT and how frequently turbulent flow approaches UPOs. Finally, we compare time-averaged properties of turbulent flows with those computed from UPOs.

A quasi-2D Kolmogorov-like flow in the experiment is generated in a shallow (6-mm-thick) electrolyte-dielectric bilayer. The fluids lie in a rectangular container with lateral (x and y) dimensions 17.8×22.9 cm² (see Fig. 1). An array of permanent magnets placed beneath the container generates a near-sinusoidal magnetic field $\mathbf{B} \sim e^{-\pi z/w} \sin(\pi y/w) \hat{z}$, where $w = 1.27$ cm is the width of each magnet. Passing a direct current ($J\hat{y}$) through the electrolyte layer generates a Lorentz force $\mathbf{F} = J\hat{y} \times \mathbf{B} \sim e^{-\pi z/w} \sin(\pi y/w) \hat{x}$ that drives a horizontal flow. The electrolyte-dielectric interface is seeded with glass microspheres and spatiotemporally resolved 2D velocity fields $\mathbf{u}(x, y, t)$ that quantify the horizontal flow are measured using particle image velocimetry [30]. Details of the experiment and DNS are provided in the Supplemental Material (SM) [31].

The quasi-2D flow in experiment is theoretically modeled using the nondimensional 2D equation [32],

$$\partial_t \mathbf{u} + \beta \mathbf{u} \cdot \nabla \mathbf{u} = -\nabla p + \frac{1}{\text{Re}} (\nabla^2 \mathbf{u} - \gamma \mathbf{u}) + \mathbf{f}, \quad (1)$$

which is derived by averaging the 3D Navier-Stokes equation in the z direction. Here, $\mathbf{u}(x, y, t)$ is assumed to be incompressible ($\nabla \cdot \mathbf{u} = 0$) and corresponds to the velocity field at the free surface in the experiment. p is

analogous to kinematic pressure. The spatial forcing profile \mathbf{f} is obtained by depth averaging and normalizing the Lorentz force \mathbf{F} . Prefactor $\beta = 0.8$ to the nonlinear term and $-\gamma \mathbf{u}$ ($\gamma = 3.86$) capture the effects due to the solid boundary at the bottom of the fluid layers. The Reynolds number Re is related to the strength of electromagnetic forcing and is the parameter used to control the complexity of flow (cf. SM [31]).

DNS of the flow governed by Eq. (1) was performed using a second-order (in space and time) finite difference code previously employed in Refs. [11,19,33]. The dimensions of the computational domain ($14w \times 18w$), no-slip velocity boundary conditions, and electromagnetic forcing in the DNS correspond to those in the experiment, facilitating direct quantitative comparison between the two. The 2D forcing profile \mathbf{f} in the DNS is antisymmetric under the inversion transformation $\mathcal{R}(x, y) \rightarrow (-x, -y)$, i.e., $\mathcal{R}\mathbf{f} = -\mathbf{f}$. Hence, Eq. (1) is equivariant under \mathcal{R} . This twofold symmetry ($\mathcal{R}^2 = \mathbb{1}$) is, however, weakly broken in experiment due to imperfections.

The Kolmogorov-like flow becomes weakly turbulent above $\text{Re} \approx 18$. Results presented in this study correspond to $\text{Re} = 23.5 \pm 1.5$ in experiment. In the DNS, turbulent time series were generated for $\text{Re} \in [22.6, 25.1]$ in steps of $\Delta \text{Re} = 0.5$. The flow is chaotic for these Re , which was validated in DNS by computing the Lyapunov exponents using continuous Gram-Schmidt orthogonalization (cf. SM [31]) [34,35]. The corresponding Kaplan-Yorke dimension is $D_{\text{KY}} \approx 12$ and the Lyapunov time is $\tau_l \approx 50$ s. We analyzed a $36\,000\tau_l$ -long turbulent time series in the DNS and experiment to detect signatures of UPOs.

Time-periodic flows are solutions to Eq. (1) that satisfy the condition $\mathbf{u}_{po}(t' + T) = \mathbf{u}_{po}(t')$. Here, t' parametrizes time along the orbit with period $T > 0$. Because of equivariance under \mathcal{R} , Eq. (1) can also possess “preperiodic” solutions such that $\mathbf{u}_{po}(t' + T) = \mathcal{R}\mathbf{u}_{po}(t')$ [26]. However, it is not known *a priori* whether UPOs of either type exist for our choice of parameters (Re , β , γ) and whether turbulent flow transiently approaches such solutions.

To identify signatures of UPOs, we performed recurrence analysis on the turbulent time series from DNS by computing [17,26]

$$r(t, \tau) = D_c^{-1} \min_g \|\mathbf{g}\mathbf{u}(t) - \mathbf{u}(t + \tau)\|, \quad g = \{\mathcal{R}, \mathbb{1}\}. \quad (2)$$

Here, $\tau > 0$ and $\|\cdot\|$ represents the L_2 norm. The normalization constant $D_c = \max_{t, \tau} \|\mathbf{u}(t) - \mathbf{u}(t + \tau)\|$ is the empirically estimated diameter of the chaotic set which ensures $r(t, \tau) \leq 1$. Low recurrence values $r(t, \tau) \ll 1$ indicate that turbulent flow fields, or their symmetry-related copies, at instants t and $t + \tau$ are similar. Therefore, during the interval $[t, t + \tau]$, the turbulent trajectory in state space is possibly near an unstable periodic or preperiodic orbit with period $T \approx \tau$. Initializing a Newton-Krylov solver [22]

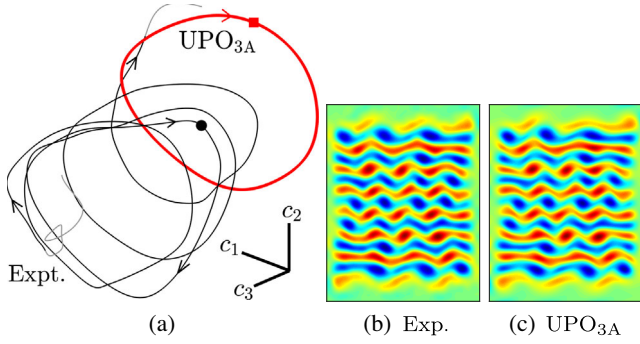


FIG. 2. (a) Low-dimensional projection of state space showing turbulent trajectory from experiment (black curve) shadowing UPO_{3A} (red loop). Each point on these curves represents a flow field. The segment in black (gray) lies in (outside) the neighborhood of UPO_{3A} . The sphere and square indicate instantaneously closest points on the turbulent trajectory and UPO_{3A} . The corresponding flow snapshots are shown in (b) and (c), where color represents vorticity $\omega = (\nabla \times \mathbf{u})_z$. The projection method is detailed in the SM [31].

with 50 initial conditions $\mathbf{u}(t)$ that correspond to deep minima in recurrence ($r \leq 0.2$), we identified seven distinct UPOs, labeled as follows: UPO_0 , UPO_1 , UPO_{2A} , UPO_{2B} , UPO_{2C} , UPO_{3A} , and UPO_{3B} . Among these, UPO_0 and UPO_1 are \mathcal{R} invariant and have been reported previously [19]. The rest lie in full state space; UPO_{2A-2C} are preperiodic orbits that lie on the same solution branch and UPO_{3B} is the symmetry-related copy of UPO_{3A} . Several properties of the UPOs are tabulated in the SM [31].

To test the dynamical relevance of a UPO in experiment, i.e., whether turbulent flows $\mathbf{u}(t)$ approach the UPO, we computed the normalized distance [19,36]:

$$D_1(t) = D_c^{-1} \min_t \|\mathbf{u}(t) - \mathbf{u}_{po}(t')\|. \quad (3)$$

D_1 is the instantaneous separation between $\mathbf{u}(t)$ and the closest point on the orbit $\mathbf{u}_{po}(t')$, as shown in Fig. 2(a). $D_1 \ll 1$ ($D_1 \approx 1$) implies the turbulent flow is very close to (far away from) the UPO in state space. We previously identified that flow fields in physical space are visually similar when $D_1 \leq 0.45$ [36]. Using this metric, we found many instances when turbulent flow approaches one of the computed UPOs. For example, Fig. 2 compares snapshots from experiment and UPO_{3A} at an instant the turbulent trajectory is near UPO_{3A} ($D_1 = 0.16$). The remarkable similarity between these flow fields confirms that turbulent trajectories in experiment indeed approach UPOs very closely.

Turbulent trajectories near a UPO should shadow its evolution in state space [7,17,18,22]. To validate this in experiment, we analyzed a particularly close pass to UPO_{3A} ; the period of this orbit is $T = 113.2$ s ($2.2\tau_l$). Using our closeness criterion, we estimated that the

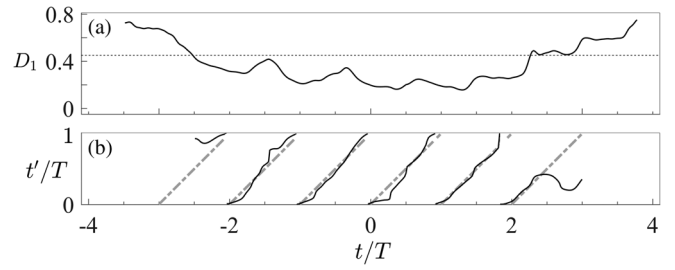


FIG. 3. (a) Instantaneous normalized separation D_1 between a turbulent trajectory in experiment and periodic orbit UPO_{3A} . The dashed black line ($D_1 = 0.45$) indicates the limit for closeness in state space. (b) t' and t parametrize time along UPO_{3A} and the turbulent trajectory, respectively. $T = 113.2$ s is the period of UPO_{3A} .

turbulent trajectory remains in the neighborhood of UPO_{3A} for a duration equal to about four periods of UPO_{3A} ($-2 < t/T < 2$ in Fig. 3). To visualize turbulent dynamics over this interval, we projected the state space around UPO_{3A} onto a low-dimensional subspace in Fig. 2. Indeed, the turbulent trajectory approaches UPO_{3A} , shadows its evolution by tracing four loops, and subsequently departs from the neighborhood of UPO_{3A} . Video 1 in the SM shows side-by-side comparison of turbulent flow and UPO_{3A} in both physical space and state space [31].

Since the shapes of the turbulent trajectory and UPO_{3A} are similar, one may ask if the corresponding flows evolve at similar rates. To explore this, for each point on the turbulent trajectory $\mathbf{u}(t)$, we identified the closest point $\mathbf{u}_{po}(t')$ on UPO_{3A} (cf. Fig. 2). We then tested whether the time t' increases at the same rate as t ; $dt'/dt = 1$ implies identical rates of evolution for the turbulent flow and the UPO it is shadowing. Figure 3(b) shows the relation between t and t' during the interval of shadowing. We defined t' on the interval $0 < t' < T$ due to periodicity of the UPO. For each of the four periods, t' (solid black line) follows the “diagonal” $t \bmod T$ (dashed gray line). This shows the turbulent trajectory and UPO_{3A} evolve at comparable rates, on average. The noticeable difference in the instantaneous rates of evolution is related to turbulent trajectories not approaching UPO_{3A} infinitesimally closely [36]. We also found that turbulent trajectories in experiment shadow UPO_0 and UPO_{2B} for a duration that is nearly 1 and 3 times their respective periods (see Figs. S2 and S3 in the SM [31]).

The statistical significance of UPOs has received little attention in previous numerical studies [29,37], and none in experiments. To address this, we computed the fraction $P(\epsilon)$ of the total time turbulent trajectories visit the ϵ neighborhood ($D_1 \leq \epsilon$) of any UPO. Figure 4(a) reveals that particularly close passes ($\epsilon \leq 0.2$) to UPOs are rare ($P < 2\%$) and require very long turbulent time series for their detection. However, increasing the size of neighborhoods to $\epsilon = 0.45$, we find that turbulent trajectories spend

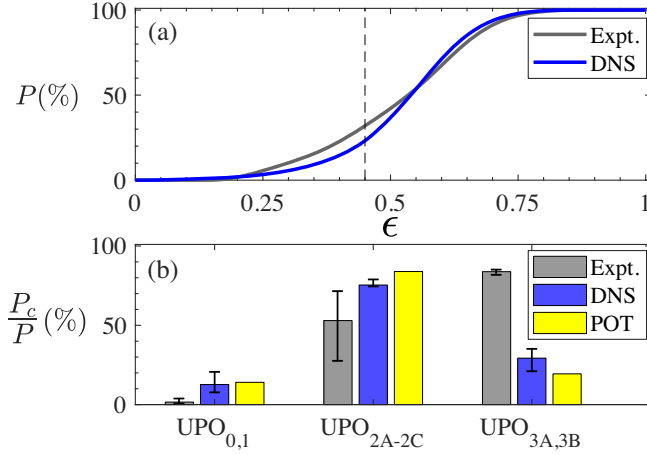


FIG. 4. Statistical significance of UPOs. (a) Probability (in %) to find a turbulent trajectory at a (normalized) distance $D_1 \leq \epsilon$ from the UPOs we computed. Dashed line indicates the upper limit $\epsilon = 0.45$ for closeness in state space. (b) Conditional probabilities for turbulent trajectories visiting neighborhoods ($\epsilon = 0.45$) of UPO clusters. Error bars indicate changes to probabilities when ϵ is varied between $[0.4, 0.5]$.

a sizable fraction of time near UPOs: about 30% in experiment and 23% in the DNS. The sensitivity of P to the choice of ϵ is comparable to that observed by Kerswell and Tutty for the statistical significance of traveling wave solutions in turbulent pipe flow at $Re = 2400$ [38].

Since very close passes to UPOs are rare, quantifying the relative importance of various UPOs required coarse partitioning of the state space. A turbulent trajectory can be simultaneously close to several UPOs which are adjacent to each other in state space. To distinguish their statistical significance, we grouped the UPOs into three clusters which are sufficiently far apart in state space: $UPO_{0,1}$, UPO_{2A-2C} , and $UPO_{3A,3B}$. These clusters were identified using pairwise separation between UPOs (cf. SM [31]). For each cluster, we then computed the conditional probability $P_c(\epsilon)/P(\epsilon)$ that a turbulent trajectory is near the UPOs in that cluster ($D_1 \leq \epsilon$), given it is near one of the seven UPOs.

The probabilities for turbulent trajectories in experiment and DNS visiting the three UPO clusters are shown in Fig. 4(b) for $\epsilon = 0.45$. Clearly, the \mathcal{R} -invariant solutions $UPO_{0,1}$ are rarely visited. In contrast, UPO clusters that do not lie in the symmetry subspace are visited frequently and hence are statistically significant. Changing the neighborhood size between $\epsilon = 0.4$ and $\epsilon = 0.5$ did not affect the results qualitatively. The discrepancy between experiments and DNS appears to be a limitation of the 2D model in reproducing some aspects of an inherently 3D laboratory flow sufficiently accurately [33].

The relative significance of UPO clusters can be rationalized using periodic orbit theory, originally developed for uniformly hyperbolic low-dimensional chaotic systems

[13,14]. The statistical “weight” associated with a UPO, and hence the probability of finding a chaotic trajectory in its infinitesimal neighborhood, is approximately given by (cf. Sec. II. 7.1 in Ref. [15])

$$\pi_i \propto \frac{1}{|\Lambda_{i1}| \cdot |\Lambda_{i2}| \cdots |\Lambda_{ik}|}, \quad (4)$$

where $|\Lambda_{i1}|, \dots, |\Lambda_{ik}|$ are the magnitudes of the unstable Floquet multipliers of UPO_i . The POT weight associated with each cluster is then $P_c/P = \sum_i \pi_i$, where the summation is over the UPOs in that cluster. The weights π_i in Eq. (4) are defined to within a normalization constant, which we chose such that the cumulative probability for the three clusters is the same for POT and DNS. Figure 4(b) shows that the statistical significance of various UPO clusters predicted using POT is fairly consistent with measurements in DNS. This is quite remarkable, given that turbulent trajectories do not visit these UPOs infinitesimally closely. Lastly, alternative weighting formulas discussed in Refs. [17,37,39,40] also yield similar estimates for the statistical significance of UPO clusters (cf. SM [31]).

The motivation behind identifying UPOs and quantifying their statistical significance is to compare statistical averages of turbulent flows with those of UPOs. Following standard practice [5,7,22], we computed the instantaneous energy input (\mathcal{I}) and dissipation (\mathcal{D}) rates,

$$\begin{aligned} \mathcal{I}(t) &= \langle \mathbf{f} \cdot \mathbf{u} \rangle_{\Omega}, \\ \mathcal{D}(t) &= -\frac{1}{Re} \langle \mathbf{u} \cdot \nabla^2 \mathbf{u} - \gamma \mathbf{u} \cdot \mathbf{u} \rangle_{\Omega}, \end{aligned} \quad (5)$$

for the turbulent flow and all the UPOs. Here, $\mathbf{a} \cdot \mathbf{b}$ is the scalar product between vector fields \mathbf{a} , \mathbf{b} and $\langle \cdot \rangle_{\Omega}$ represents the integral $\int_{\Omega} (\dots) dx dy$ evaluated over the entire flow domain Ω . In Fig. 5, we plotted the difference between instantaneous input and dissipation rates ($\mathcal{I} - \mathcal{D}$) versus the energy input rate \mathcal{I} for the turbulent flow in experiment. \mathcal{I} and \mathcal{D} are normalized by the temporal mean $\langle \mathcal{I} \rangle_t = \langle \mathcal{D} \rangle_t$. The corresponding quantities for each UPO are overlaid. Additionally, the probability density function for \mathcal{I} from experiment (as well as DNS) is shown in the inset.

For the statistically significant UPO_{2A-2C} and $UPO_{3A,3B}$, both energy input and dissipation rates cluster around the turbulent mean values, located at $\mathcal{I}/\langle \mathcal{I} \rangle_t = 1$ and $\mathcal{I} - \mathcal{D} = 0$ in Fig. 5. The \mathcal{I} (and \mathcal{D}) values for these UPOs vary over a narrow range (0.95, 1.07) that is approximately $\pm \sigma_{\mathcal{I}}$ of the turbulent mean, where $\sigma_{\mathcal{I}} = 0.055$ is the standard deviation of \mathcal{I} for turbulent flow. Consequently, the mean energy input (and dissipation) rate for each of these five UPOs is within $\pm 0.6\sigma_{\mathcal{I}}$ of the turbulent average (unity), as shown in the inset. In contrast, $UPO_{0,1}$, which are statistically insignificant, have mean values of \mathcal{I} and \mathcal{D} that deviate by over $2\sigma_{\mathcal{I}}$ from the turbulent mean value.

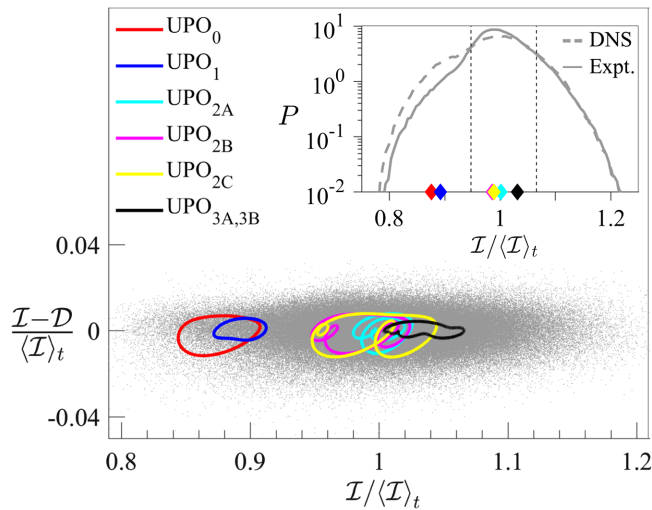


FIG. 5. Energy input rate \mathcal{I} versus the difference between input and dissipation rates $(\mathcal{I} - \mathcal{D})$ for turbulent time series in experiment (scatter plot) and UPOs (closed loops). Inset: Probability density function of $\mathcal{I}(t)$ for turbulent flow in experiment (solid gray curve) and DNS (dashed gray curve). Colored symbols show the mean values of \mathcal{I} for each of the seven UPOs and the dashed black lines represent the range of \mathcal{I} for UPO_{2A-2C} and UPO_{3A,3B}.

In this Letter, we provided unambiguous experimental evidence for the dynamical relevance and statistical significance of UPOs in a moderately turbulent flow. We showed that turbulent trajectories in state space transiently approach UPOs closely and shadow their spatiotemporal evolution. We also quantified the statistical significance of various UPOs by computing the fraction of time turbulent trajectories visit their neighborhoods. The estimates from DNS are consistent with the “weights” predicted by periodic orbit theory. Lastly, we showed that statistically significant UPOs capture time-averaged properties of the turbulent flows in both experiment and DNS accurately.

Our study identified that turbulent flows spend about 30% of the time near the UPOs we computed. This suggests that UPOs with longer periods as well as other types of nonchaotic solutions—such as unstable equilibria, quasiperiodic orbits, and heteroclinic or homoclinic connections—may also play an important dynamical and statistical role [10,24,41,42]. Their existence and dynamical relevance, at least in symmetry-invariant subspaces, was recently demonstrated for both 2D and 3D shear flows [10,19,41,42]. Hence, a dynamical framework based on UPOs, as well as other types of recurrent solutions, should ultimately enable forecasting [11,36] and control (e.g., Lüthje *et al.* [43]) of turbulent dynamics, besides accurately predicting its statistical properties.

M. F. S. and R. O. G. acknowledge funding from the National Science Foundation (CMMI-1234436, DMS-1125302, CMMI-1725587) and Defense Advanced Research Projects Agency (HR0011-16-2-0033). B. S.

has received funding from the People Programme (Marie Curie Actions) of the European Union's Seventh Framework Programme FP7/2007–2013/ under REA Grant Agreement No. 291734.

*bsuri@ist.ac.at

†roman.grigoriev@physics.gatech.edu

‡michael.schatz@physics.gatech.edu

- [1] B. Hof, C. W. H. van Doorne, J. Westerweel, F. T. M. Nieuwstadt, H. Faisst, B. Eckhardt, H. Wedin, R. R. Kerswell, and F. Waleffe, Experimental observation of nonlinear traveling waves in turbulent pipe flow, *Science* **305**, 1594 (2004).
- [2] S. K. Robinson, Coherent motions in the turbulent boundary layer, *Annu. Rev. Fluid Mech.* **23**, 601 (1991).
- [3] D. J. C. Dennis and F. M. Sogaro, Distinct Organizational States of Fully Developed Turbulent Pipe Flow, *Phys. Rev. Lett.* **113**, 234501 (2014).
- [4] G. Boffetta and R. E. Ecke, Two-dimensional turbulence, *Annu. Rev. Fluid Mech.* **44**, 427 (2012).
- [5] L. van Veen, A. Vela-Martin, and G. Kawahara, Time-Periodic Inertial Range Dynamics, *Phys. Rev. Lett.* **123**, 134502 (2019).
- [6] S. Goto, Coherent structures and energy cascade in homogeneous turbulence, *Prog. Theor. Phys. Suppl.* **195**, 139 (2012).
- [7] G. Kawahara and S. Kida, Periodic motion embedded in plane Couette turbulence: regeneration cycle and burst, *J. Fluid Mech.* **449**, 291 (2001).
- [8] J. F. Gibson, J. Halcrow, and P. Cvitanović, Visualizing the geometry of state space in plane Couette flow, *J. Fluid Mech.* **611**, 107 (2008).
- [9] A. de Lozar, F. Mellibovsky, M. Avila, and B. Hof, Edge State in Pipe Flow Experiments, *Phys. Rev. Lett.* **108**, 214502 (2012).
- [10] M. Avila, F. Mellibovsky, N. Roland, and B. Hof, Streamwise-Localized Solutions at the Onset of Turbulence in Pipe Flow, *Phys. Rev. Lett.* **110**, 224502 (2013).
- [11] B. Suri, J. Tithof, R. O. Grigoriev, and M. F. Schatz, Forecasting Fluid Flows Using the Geometry of Turbulence, *Phys. Rev. Lett.* **118**, 114501 (2017).
- [12] E. Hopf, A mathematical example displaying features of turbulence, *Commun. Pure Appl. Math.* **1**, 303 (1948).
- [13] D. Auerbach, P. Cvitanović, J. P. Eckmann, G. Gunaratne, and I. Procaccia, Exploring Chaotic Motion Through Periodic Orbits, *Phys. Rev. Lett.* **58**, 2387 (1987).
- [14] P. Cvitanović, Invariant Measurement of Strange Sets in Terms of Cycles, *Phys. Rev. Lett.* **61**, 2729 (1988).
- [15] Y. Lan, Cycle expansions: From maps to turbulence, *Commun. Nonlinear Sci. Numer. Simul.* **15**, 502 (2010).
- [16] J. F. Gibson, Channelflow: A spectral Navier-Stokes simulator in C++, Technical Report, University of New Hampshire, 2014, <http://channelflow.org/dokuwiki/doku.php?id=citation>.
- [17] G. J. Chandler and R. R. Kerswell, Invariant recurrent solutions embedded in a turbulent two-dimensional Kolmogorov flow, *J. Fluid Mech.* **722**, 554 (2013).

- [18] N. B. Budanur, K. Y. Short, M. Farazmand, A. P. Willis, and P. Cvitanović, Relative periodic orbits form the backbone of turbulent pipe flow, *J. Fluid Mech.* **833**, 274 (2017).
- [19] B. Suri, R. K. Pallantla, M. F. Schatz, and R. O. Grigoriev, Heteroclinic and homoclinic connections in a Kolmogorov-like flow, *Phys. Rev. E* **100**, 013112 (2019).
- [20] E. J. Kostelich, I. Kan, C. Grebogi, E. Ott, and J. A. Yorke, Unstable dimension variability: A source of nonhyperbolicity in chaotic systems, *Physica (Amsterdam)* **109D**, 81 (1997).
- [21] S. Toh and T. Itano, A periodic-like solution in channel flow, *J. Fluid Mech.* **481**, 67 (2003).
- [22] D. Viswanath, Recurrent motions within plane Couette turbulence, *J. Fluid Mech.* **580**, 339 (2007).
- [23] Y. Duguet, C. C. T. Pringle, and R. R. Kerswell, Relative periodic orbits in transitional pipe flow, *Phys. Fluids* **20**, 114102 (2008).
- [24] L. van Veen and G. Kawahara, Homoclinic Tangle on the Edge of Shear Turbulence, *Phys. Rev. Lett.* **107**, 114501 (2011).
- [25] T. Kreilos and B. Eckhardt, Periodic orbits near onset of chaos in plane Couette flow, *Chaos* **22**, 047505 (2012).
- [26] A. P. Willis, P. Cvitanović, and M. Avila, Revealing the state space of turbulent pipe flow by symmetry reduction, *J. Fluid Mech.* **721**, 514 (2013).
- [27] J. Page and R. R. Kerswell, Searching turbulence for periodic orbits with dynamic mode decomposition, *J. Fluid Mech.* **886**, A28 (2020).
- [28] F. Waleffe, On a self-sustaining process in shear flows, *Phys. Fluids* **9**, 883 (1997).
- [29] D. Lucas and R. R. Kerswell, Recurrent flow analysis in spatiotemporally chaotic 2-dimensional Kolmogorov flow, *Phys. Fluids* **27**, 045106 (2015).
- [30] B. Drew, J. Charonko, and P. P. Vlachos, QI—Quantitative imaging (PIV and more) (2013), <https://sourceforge.net/projects/qi-tools/>.
- [31] See Supplemental Material at <http://link.aps.org/supplemental/10.1103/PhysRevLett.125.064501> for details regarding (i) experimental setup, (ii) DNS, (iii) D_{KY} computation, (iv) properties of UPOs, (v) state space projection procedure, (vi) turbulent trajectories shadowing UPO_0 and UPO_{2B} , (vii) pairwise separation between UPOs, and (viii) comparison of UPO weighting protocols. Videos 1, 2, and 3 show side-by-side comparison of turbulent flows in experiment shadowing UPO_{3A} , UPO_0 , and UPO_{2B} , respectively.
- [32] B. Suri, J. Tithof, R. Mitchell, R. O. Grigoriev, and M. F. Schatz, Velocity profile in a two-layer Kolmogorov-like flow, *Phys. Fluids* **26**, 053601 (2014).
- [33] J. Tithof, B. Suri, R. K. Pallantla, R. O. Grigoriev, and M. F. Schatz, Bifurcations in a quasi-two-dimensional Kolmogorov-like flow, *J. Fluid Mech.* **828**, 837 (2017).
- [34] D. A. Egolf, I. V. Melnikov, W. Pesch, and R. E. Ecke, Mechanisms of extensive spatiotemporal chaos in Rayleigh–Bénard convection, *Nature (London)* **404**, 733 (2000).
- [35] A. Karimi and M. R. Paul, Quantifying spatiotemporal chaos in Rayleigh–Bénard convection, *Phys. Rev. E* **85**, 046201 (2012).
- [36] B. Suri, J. Tithof, R. O. Grigoriev, and M. F. Schatz, Unstable equilibria and invariant manifolds in quasi-two-dimensional Kolmogorov-like flow, *Phys. Rev. E* **98**, 023105 (2018).
- [37] E. Kazantsev, Unstable periodic orbits and attractor of the barotropic ocean model, *Nonlinear Processes Geophys.* **5**, 193 (1998).
- [38] R. R. Kerswell and O. R. Tutty, Recurrence of travelling waves in transitional pipe flow, *J. Fluid Mech.* **584**, 69 (2007).
- [39] S. M. Zoldi and H. S. Greenside, Spatially localized unstable periodic orbits of a high-dimensional chaotic system, *Phys. Rev. E* **57**, R2511 (1998).
- [40] S. M. Zoldi, Unstable Periodic Orbit Analysis of Histograms of Chaotic Time Series, *Phys. Rev. Lett.* **81**, 3375 (1998).
- [41] T. M. Schneider, B. Eckhardt, and J. Vollmer, Statistical analysis of coherent structures in transitional pipe flow, *Phys. Rev. E* **75**, 066313 (2007).
- [42] M. Farano, S. Cherubini, J.-C. Robinet, P. De Palma, and T. M. Schneider, Computing heteroclinic orbits using adjoint-based methods, *J. Fluid Mech.* **858**, R3 (2018).
- [43] O. Lüthje, S. Wolff, and G. Pfister, Control of Chaotic Taylor-Couette Flow with Time-Delayed Feedback, *Phys. Rev. Lett.* **86**, 1745 (2001).